Lecture 1 : Macroscopic Characterisation of Soils

Kenichi Soga, University of Cambridge

1.1 Introduction

All aspects of soil stability—bearing capacity, slope stability, the supporting capacity of deep foundations, and penetration resistance, to name a few—depend on soil strength. The stress-deformation and stress-deformation-time behaviour of soils are important in any problem where ground movements are of interest. Most relationships for the characterization of the stress-deformation and strength properties of soils are empirical and based on phenomenological descriptions of soil behaviour. The Mohr–Coulomb equation is by far the most widely used for strength. It states that

$$\tau_{ff} = c + \sigma_{ff} \tan\phi \tag{1.1}$$

$$\tau_{ff} = c' + \sigma'_{ff} \tan\phi' \tag{1.2}$$

where τ_{ff} is shear stress at failure on the failure plane, c is a cohesion intercept, σ_{ff} is the normal stress on the failure plane, and ϕ is a friction angle. Equation (1.1) applies for σ_{ff} defined as a total stress, and c and ϕ are referred to as total stress parameters. Equation (1.2) applies for σ'_{ff} defined as an effective stress, and c' and ϕ' are effective stress parameters. As the shear resistance of soil originates mainly from actions at interparticle contacts, the second equation is the more fundamental.

In reality, the shearing resistance of a soil depends on many factors, and a complete equation might be of the form

$$\text{Shearing resistance} = F(e, c', \phi', \sigma', C, H, T, \varepsilon, \dot{\varepsilon}, S) \tag{1.3}$$

in which e is the void ratio, C is the composition, H is the stress history, T is the temperature, ε is the strain, $\dot{\varepsilon}$ is the strain rate, and S is the structure. All parameters in these equations may not be independent, and the functional forms of all of them are not known. Consequently, the shear resistance values (including c' and ϕ') are determined using specified test type (i.e., direct shear, triaxial compression, simple shear), drainage conditions, rate of loading, range of confining pressures, and stress history. As a result, different friction angles and cohesion values have been defined, including parameters for total stress, effective stress, drained, undrained, peak strength, and residual strength. The shear resistance values applicable in practice depend on factors such as whether or not the problem is one of loading or unloading, whether or not short-term or long-term stability is of interest, and stress orientations.

1.2 General Characteristics of strength and deformation

1. In the absence of chemical cementation between grains, the strength (stress state at failure or the ultimate stress state) of sand and clay is approximated by a linear relationship with stress.

$$\tau_{ff} = \sigma'_{ff} \tan\phi' \qquad \text{or} \tag{1.4}$$

$$(\sigma'_{1ff} - \sigma'_{3ff}) = (\sigma'_{1ff} + \sigma'_{3ff})\sin\phi' \qquad (1.5)$$

where the primes designate effective stresses and σ'_{1ff} and σ'_{3ff} are the major and minor principal effective stresses at failure, respectively.

2. The basic contributions to soil strength are frictional resistance between soil particles in contact and internal kinematic constraints of soil particles associated with changes in the soil fabric. The magnitude of these contributions depends on the effective stress and the volume change tendencies of the soil. For such materials the stress-strain curve from a shearing test is typically of the form shown in Fig. 1.1(a). The maximum or peak strength of a soil (point b) may be greater than the critical state strength, in which the soil deforms under sustained loading at constant volume (point c). For some soils, the particles align along a localized failure plane after large shear strain or shear displacement, and the strength decreases even further to the residual strength (point d). The corresponding three failure envelopes can be defined as shown in Fig. 1.1(b), with peak, critical and residual friction angles (or states) as indicated.

3. Peak failure envelopes are usually curved in the manner shown schematically in Fig. 1.1(b). This behavior is caused by dilatancy suppression and grain crushing at higher stresses. Curved failure envelopes are also observed for many clays at residual state.

4. The peak strength of cohesionless soils is influenced most by density, effective confining pressures, test type and sample preparation methods. For dense sand, the 'secant' peak friction angle (point b in Fig. 1.1(b)) consists in part of internal rolling and sliding friction between grains and in part of interlocking of particles (Taylor, 1948). The interlocking necessitates either volume expansion (dilatancy) or grain fracture and/or crushing if there is to be deformation. For loose sand, the peak friction angle (point b' in Fig.1.1(b)) normally coincides with the critical state friction angle (point c'), and there is no peak in the stress-strain curve.

5. The peak strength of saturated clay is influenced most by overconsolidation ratio, drainage conditions, effective confining pressures, original structure, disturbance (which causes a change in effective stress and a loss of cementation), and creep or deformation rate effects. Overconsolidated clays usually have higher peak strength at a given effective stress than normally consolidated clays, as shown in Fig. 1.2. The differences in strength result from both the different stress histories and the different water contents at peak. For comparisons at the same water content but different effective stress, as for points A and A′, the Hvorslev strength parameters c_e and ϕ_e are obtained (Hvorslev, 1937, 1960).

6. During critical state deformation a soil is completely destructured. As illustrated in Fig. 1.1(b), the critical state friction angle values are independent of stress history and original structure; for a given set of testing conditions the

shearing resistance depends only on composition and effective stress. The basic concept of the critical state is that under sustained uniform shearing at failure, there exists a unique combination of void ratio e, mean pressure p' and deviator stress q. [1] The critical states of reconstituted Weald clay and Toyoura sand are shown in Fig.1.3. The critical state line on the p'-q plane is linear[2], whereas that on an e-lnp' (or e-log p') plane tends to be linear for clays and nonlinear for sands.

7. At failure, dense sands and heavily overconsolidated clays have a greater volume after drained shear or a higher effective stress after undrained shear than at the start of deformation. This is due to its dilative tendency upon shearing. At failure, loose sands and normally consolidated-to-moderately overconsolidated clays (OCR up to about 4) have a smaller volume after drained shear or a lower effective stress after undrained shear than they had initially. This is due to its contractive tendency upon shearing.

8. Under further deformation, platy clay particles begin to align along the failure plane and the shear resistance may further decrease from the critical state condition. The angle of shear resistance at this condition is called the residual friction angle, as illustrated in Fig. 1.1(b). The post-peak shearing displacement required to cause a reduction in friction angle from the critical state value to the residual value varies with the soil type, normal stress on the shear plane, and test conditions. For example, for shale mylonite[3] in contact with smooth steel or other polished hard surfaces, a shearing displacement of only 1 or 2 mm is sufficient to give residual strength. For soil against soil, a slip along the shear plane of several tens of mm may be required, as shown by Fig. 1.4. However, significant softening can be caused by strain localization and development of shear bands, especially for dense samples under low confinement.

---

[1] In three dimensional stress space $\sigma' = (\sigma_x', \sigma_y', \sigma_z', \tau_{xy}, \tau_{yz}, \tau_{zx})$ or the equivalent principle stresses ($\sigma_1', \sigma_2' \sigma_3'$), the mean effective stress p' and the deviator stress q is defined as

$$p' = (\sigma'_x + \sigma'_y + \sigma'_z)/3 = (\sigma'_1 + \sigma'_2 + \sigma'_3)/3$$

$$q = (1/\sqrt{2})\sqrt{(\sigma'_x - \sigma'_y)^2 + (\sigma'_y - \sigma'_z)^2 + (\sigma'_z - \sigma'_x)^2 + 6\tau_{xy}^2 + 6\tau_{yz}^2 + 6\tau_{zx}^2}$$
$$= (1/\sqrt{2})\sqrt{(\sigma'_1 - \sigma'_2)^2 + (\sigma'_2 - \sigma'_3)^2 + (\sigma'_3 - \sigma'_1)^2}$$

For triaxial compression condition ($\sigma_1' > \sigma_2' = \sigma_3'$), $p' = (\sigma_1' + 2\sigma_2')/3$, $q = \sigma_1' - \sigma_2'$

[2] The critical state failure slope on p'-q plane is related to friction angle ϕ', as described later.

[3] A rock that has undergone differential movements at high temperature and pressure in which the mineral grains are crushed against one another. The rock shows a series of lamination planes.

9. Strength anisotropy may result from both stress and fabric anisotropy. In the absence of chemical cementation, the differences in the strength of two samples of the same soil at the same void ratio but with different fabrics are accountable in terms of different effective stresses.

10. Undrained strength in triaxial compression may differ significantly from the strength in triaxial extension. However, the influence of type of test (triaxial compression versus extension) on the effective stress parameters c' and ϕ' is relatively small. Effective stress friction angles measured in plane strain are typically about 10 percent greater than those determined by triaxial compression.

11. A change in temperature causes either a change in void ratio or a change in effective stress (or a combination of both) in saturated clay. Thus, a change in temperature can cause a strength increase or a strength decrease, depending on the circumstances, as illustrated by Figs. 1.5. For the tests on kaolinite shown in Fig. 1.5, all samples were prepared by isotropic triaxial consolidation at 75 °F. Then, with no further drainage allowed, temperatures were increased to the values indicated, and the samples were tested in unconfined compression. Substantial reductions in strength accompanied the increases in temperature.

Stress-Strain Behavior

1. Stress-strain behavior ranges from very brittle for some quick clays, cemented soils, heavily overconsolidated clays, and dense sands, to ductile for insensitive and remolded clays and loose sands, as illustrated by Fig. 1.6. An increase in confining pressure causes an increase in the deformation modulus as well as an increase in strength, as shown by Fig. 1.7.

2. Stress-strain relationships are usually nonlinear; soil stiffness (often expressed in terms of tangent or secant modulus) generally decreases with increasing shear strain or stress level up to peak failure stress. Fig. 1.8 shows a typical stiffness degradation curve, in terms of shear modulus G and Young's modulus E, along with typical strain levels developed in geotechnical construction (Mair, 1993) and as associated with different laboratory testing techniques used to measure the stiffness (Atkinson, 2000). For example, Fig. 1.9 shows the stiffness degradation of sands and clay subjected to increase in shear strain. As illustrated in Fig. 1.9, the stiffness degradation curve can be separated into four zones; (1) linear elastic zone, (2) nonlinear elastic zone, (3) pre-yield plastic zone and (4) full plastic zone.

3 In the linear elastic zone, soil particles do not slide relative to each other under a small stress increment, and the stiffness is at its maximum. The soil stiffness depends on contact interactions, particle packing arrangement and elastic stiffness of the solids. Low strain stiffness values can be determined using elastic wave velocity measurements, resonant column testing or local strain transducer measurements. The magnitudes of the small strain shear modulus (G_{max}) and Young's modulus (E_{max}) depend on applied confining pressure and

the packing conditions of soil particles. The following empirical equations are often employed to express these dependencies.

$$G_{\max} = A_G F_G(e) p'^{n_G} \tag{1.6}$$

$$E_{i(\max)} = A_E F_E(e) \sigma'^{n_E}_i \tag{1.7}$$

where $F_G(e)$ and $F_E(e)$ are functions of void ratio, p' is the mean effective confining pressure, σ'_i is the effective stress in the i-direction, and the other parameters are material constants. Figure 1.10 shows examples of the fitting of the above equations to experimental data.

4. The stiffness begins to decrease from the linear elastic value as the applied strains or stresses increase, and the deformation moves into the nonlinear elastic zone. However, a complete cycle of loading, unloading and reloading within this zone shows full recovery of strains. The strain at the onset of the nonlinear elastic zone ranges from less than 5×10^{-4} % for non-plastic soils at low confining pressure conditions to greater than 5×10^{-2} % at high confining pressure or in soils with high plasticity (Santamarina et al., 2000).

5. Irrecoverable strains develop in the pre-yield plastic zone. The initiation of plastic strains can be determined by examining the onset of permanent volumetric strain in drained conditions or residual excess pore pressures in undrained conditions after unloading. Available experimental data suggest that the strain level that initiates plastic strains ranges between 7×10^{-3} and 7×10^{-2} %, with the lower limit for uncemented normally consolidated sands and the upper limit for high plasticity clays and cemented sands.

6. A distinctive kink in the stress-strain relationship defines yielding, beyond which full plastic strains are generated. A locus of stress states that initiate yielding defines the yield envelope. Typical yield envelopes for sand and natural clay are shown in Fig. 1.11. The yield envelope expands, shrinks and rotates as plastic strains develop. It is usually considered that expansion is related to plastic volumetric strains; the surface expands when the soil compresses and shrinks when the soil dilates. The two inner envelopes shown in Fig. 1.11(b) define the boundaries between linear elastic, nonlinear elastic, and pre-yield zones. When the stress state moves in the pre-yield zone, the inner envelopes move with the stress state. This multi-envelope concept allows modeling of complex deformations observed for different stress paths (Mroz, 1967; Prevost, 1977; Dafalias and Herrman, 1982; Atkinson et al., 1990; Jardine, 1992).

7. Plastic irrecoverable shear deformations of saturated soils are accompanied by volume changes when drainage is allowed or changes in pore water pressure and effective stress when drainage is prevented. The general nature of this

behavior is shown in Fig. 1.12(a) and (b) for drained and undrained conditions, respectively. The volume and pore water pressure changes depend on interactions between fabric and stress state and the ease with which shear deformations can develop without overall changes in volume or transfer of normal stress from the soil structure to the pore water.

8. The stress-strain relation of clays depends largely on overconsolidation ratio, effective confining pressures and drainage conditions. Fig. 1.13 shows triaxial compression behavior of clay specimens that are first normally consolidated and then isotropically unloaded to different overconsolidation ratios before shearing. The specimens are consolidated at the same confining pressure p_0', but have different void ratios due to the different stress history (Fig. 1.13a). Drained tests on normally consolidated clays and lightly overconsolidated clays show ductile behavior with volume contraction (Fig. 1.13b). Heavily overconsolidated clays exhibit a stiff response initially until the stress state reaches the yield envelope giving the peak strength and volume dilation. The state of the soil then progressively moves towards the critical state exhibiting softening behavior. Undrained shearing of normally consolidated and lightly overconsolidated clays generates positive excess pore pressures, whereas shear of heavily overconsolidated clays generates negative excess pore pressures (Fig. 1.13c).

9. The magnitudes of pore pressure that are developed in undrained loading depend on initial consolidation stresses, overconsolidation ratio, density and soil fabric. Fig. 1.14 shows the undrained effective stress paths of anisotropically and isotropically consolidated specimens (Ladd and Varallyay, 1965). The difference in undrained shear strength is primarily due to different excess pore pressure development associated with the change in soil fabric. At large strains, the stress paths correspond to the same friction angle.

10. A temperature increase causes a decrease in undrained modulus; that is, a softening of the soil. As an example, initial strain as a function of stress is shown in Fig. 1.15 for Osaka clay tested in undrained triaxial compression at different temperatures. Increase in temperature causes consolidation under drained conditions and softening under undrained conditions.

1.3 Critical State: A Useful Reference Condition

After large shear induced volume change, a soil under a given effective confining stress will arrive ultimately at a unique final water content or void ratio that is independent of its initial state. At this stage, the interlocking achieved by densification or overconsolidation is gone in the case of dense soils, the metastable structure of loose soils has collapsed, and the soil is fully destructured. A well defined strength value is reached at this state, and this is often referred to as the *critical state strength*. Under undrained conditions, the critical state is reached when the pore pressure and the effective stress remain constant during continued deformation. The critical state can be considered a fundamental state, and it can be used as a reference state to explain the effect of overconsolidation ratios, relative density and different stress paths on strength properties of soils (Schofield and Wroth, 1968).

Clays

The basic concept of the critical state is that, under sustained uniform shearing, there exists a unique relationships among void ratio e_{cs} (or specific volume $v_{cs} = 1 + e_{cs}$), mean effective pressure p'_{cs}, and deviator stress q_{cs} as shown in Fig.1.16. An example of the critical state of clay was shown in Fig. 1.3(a). The critical state of clay can be expressed as

$$q_{cs} = Mp'_{cs} \tag{1.8}$$

$$v_{cs} = 1 + e_{cs} = \Gamma - \lambda_{cs} \ln p'_{cs} \tag{1.9}$$

where q_{cs} is the deviator stress at failure and p'_{cs} is the mean effective stress at failure and M is the critical state stress ratio. The critical state on the void ratio (or specific volume) – mean pressure plane is defined by two material parameters: λ_{cs}, the critical state compression index and Γ, the void ratio or specific volume intercept at unit pressure ($p' = 1$). The compression lines under constant stress ratios are often parallel to each other, as shown in Fig. 1.16.

Parameter M in equation (1.8) defines the critical state stress ratio at failure, and is similar to ϕ' for the Mohr-Coulomb failure line. However, equation (1.8) includes the effect of intermediate principal stress σ'_2 because $p' = \sigma_1' + \sigma_2' + \sigma_3'$, whereas, the Mohr coulomb failure criterion of equation (1.4) or (1.5) does not take the intermediate effective stress into account. In triaxial conditions, $\sigma'_a > \sigma'_r = \sigma'_r$ and $\sigma'_r = \sigma'_r > \sigma'_a$ for compression and extension, respectively (see Fig. 1.16). Hence, equations (1.4) and (1.8) can be related to each other for these two cases as follows.

$$M = \frac{6\sin\phi'_{crit}}{3 - \sin\phi'_{crit}} \quad \text{for triaxial compression} \tag{1.10}$$

$$M = \frac{6\sin\phi'_{crit}}{3 + \sin\phi'_{crit}} \quad \text{for triaxial extension} \tag{1.11}$$

These equations indicate that the correlation between M and ϕ'_{crit} is not unique but depends on the stress conditions. Neither is a fundamental property of the soil. Nonetheless, both are widely used in engineering practice, and if interpreted properly, they can provide useful and simple phenomenological representations of complex behavior.

The drained and undrained critical state strengths are illustrated in Fig. 1.17(a) and (b) for normally consolidated clay and heavily overconsolidated clay, respectively. The initial mean pressure-void ratio state of the normally consolidated clay is above the critical state line, whereas that of the heavily overconsolidated clay is below the critical state line. When the initial state of the soil is normally consolidated at A (Fig. 1.17(a)), the critical state is B for undrained loading and C for drained triaxial compression. Hence, the deviator stress at critical state is smaller for the undrained case than for the drained case. On the other hand, when the initial state of the soil is overconsolidated at D (Fig. 1.17(b)), the critical state becomes E for undrained loading and F for drained triaxial compression. The deviator stress at critical state is smaller for the drained case compared to the undrained case. It is important to note that the soil state needs to satisfy both state equations (equations (1.8) and (1.9)) to be at critical state.

For example, point G in Fig. 1.17(b) satisfies (p'_{cs} and q_{cs}), but not e_{cs}; therefore, it is not at the critical state.

Converting the void ratio in equation (1.9) to water content, a normalized critical state line can be written using the liquidity index (see Fig. 1.18).

$$LI_{CS} = \frac{w_{CS} - w_{PL}}{w_{LL} - w_{PL}} = \frac{\ln(p_{PL}'/p')}{\ln(p'_{PL}/p'_{LL})} \tag{1.12}$$

where w_{cs} is the water content at critical state when the effective mean pressure is p'. p'_{LL} and p'_{PL} are the mean effective pressure at liquid limit (w_{LL}) and plastic limit (w_{PL}), respectively. $p'_{LL} \approx$ 1.5-6 kPa and $p'_{PL} \approx$ 150-600 kPa are expected considering the undrained shear strengths at liquid and plastic limits are in the ranges c_{uLL} = 1-3 kPa and c_{uPL} = 100-300 kPa, respectively[4].

Using equation (1.12), a relative state in relation to the critical state for a given effective mean pressure (i.e. above or below the critical state line) can be defined as (see Fig. 1.18)

$$LI_{eq} = LI - LI_{CS} + 1 = LI + \frac{\log(p'/p'_{LL})}{\log(p'_{PL}/p'_{LL})} \tag{1.13}$$

where LI_{eq} is the equivalent liquidity index defined by Schofield (1980). When LI_{eq} = 1 (i.e. $LI = LI_{CS}$) and $q/p' = M$, the clay has reached the critical state. Fig. 1.19 gives the stress ratio when plastic failure (or fracture) initiates at a given water content. When LI_{eq}>1 (the state is above the critical state line), and the soil in a plastic state exhibits uniform contractive behavior. When LI_{eq}<1 (the state is below the critical state line), and the soil in a plastic state exhibits localized dilatant rupture, or possibly fracture, if the stress ratio reaches the tensile limit (q/p' = 3 for triaxial compression and -1.5 for triaxial extension, see Fig. 1.19(b)). Hence, the critical state line can be used as a reference to characterize possible soil behavior under plastic deformation.

Sands

The critical state strength and relative density of sand can be expressed as

$$q_{cs} = Mp'_{cs} \tag{1.14}$$

$$D_{R,cs} = \frac{e_{\max} - e_{cs}}{e_{\max} - e_{\min}} = \frac{1}{\ln(\sigma_c / p')} \tag{1.15}$$

---

[4] A review by Sharma and Bora (2003) gives average values of c_{uLL} = 1.7 kPa and c_{uPL} = 170 kPa.

where e_{cs} is the void ratio at critical state, e_{max} and e_{min} are the maximum and minimum void ratios and σ_c is the crushing strength of the particles[5]. The critical state line based on equation (1.15) is plotted in Fig. 1.20. The plotted critical state lines are non-linear in the *e-lnp′* plane as shown in Fig. 1.20(a), in contrast to the linear relationship found for clays. This nonlinearity is confirmed by experimental data as shown in Fig. 1.20(b). However, this nonlinearity can be considered as an artifact when the data are plotted in a normal *e-p′* plane as shown in Figure 1.20(b). The critical state line is more or less a straight line in this plane.

At high confining pressure, when the effective mean pressure becomes larger than the crushing strength, many particles begin to break and the lines become more or less linear in the *e-lnp′* plane, similar to the behavior of clays. Coop and Lee (1993) found that there is a unique relationship between the amount of particle breakage that occurred on shearing to a critical state and the value of the mean normal effective stress. This implies that sand at the critical state would reach a stable grading at which the particle contact stresses would not be sufficient to cause further breakage. Coop et al. (2004) performed ring shear tests on a carbonate sand to find a shear strain required to reach the true critical state (i.e. constant particle grading). They found that particle breakage continues to very large strains, far beyond those reached in triaxial tests. Fig. 1.21(a) shows the volumetric strains measured for a selection of their tests, which were carried out at vertical stress levels in the range of 650-860 kPa. A constant volumetric strain is reached at a shear strain of around 2000%. For specimens at lower stress levels, more shear strains (20,000% or more) were required. Similar findings were made for quartz sand (Luzzani and Coop, 2002). Fig. 1.21(b) shows the degree of particle breakage with shear strains in the logarithmic scale. The amount of breakage is quantified by Hardin's (1985) relative breakage parameter *Br*. At very large strains, the value of *Br* finally stabilizes. The strain required for stabilization depends on applied stress level. Interestingly, less shear strain was needed for the mobilized friction angle to reach the steady state value (Fig. 1.21 (c)) than for attainment of the constant volume condition, (Fig. 1.21 (a)). The critical state friction angle was unaffected by the particle breakage.

In summary, the critical state concept is very useful to characterize the strength and deformation properties of soils when it is used as a reference state. That is, a soil has a tendency to contract upon shearing when its state is above the critical state line, whereas it has a tendency to dilate when it is below the critical state line. Various normalized state parameters have been proposed to characterize the difference between the actual state and the critical state line, as illustrated in Fig. 1.22.

---

[5] Equation 1.15 is derived from equation 1.19 proposed by Bolton (1986) with $I_R = 0$ (zero dilation). Bolton's equation is discussed later. Other mathematical expressions to fit the experimentally determined critical state line are possible. For example, Li et al. (1999) propose the following equation for the critical state line (e_{cs} versus p').

$$e_{cs} = e_0 - \lambda_s \left(\frac{p'}{p_a} \right)^{\xi}$$

where e_0 is the void ratio at $p = 0$, p_a is atmospheric pressure, and λ_s and ξ are material constants.

1.4 Strength Parameters for Sands

Many factors and phenomena act together to determined the shearing resistance of sands; e.g. mineralogy, grain size, grain shape, grain size distribution, (relative) density, stress state, type of tests and stress path, drainage, etc (see equation (1.3)). In this section, the ways in which these factors have become understood and have been quantified over the last several decades are summarized. Several correlations are given to provide an overview and reference for typical values and ranges of strength parameters for sands and the influences of various factors on these parameters[6].

Early Studies

The important role of volume change during shear, especially dilatancy, was recognized by Taylor (1948). From direct shear box testing of dense sand specimens, he calculated the work at peak shear stress state and showed that the energy input is dissipated by the friction using the following equation.

$$\tau_{peak} dx - \sigma'_n dy = \mu \sigma'_n dx \tag{1.16}$$

where τ_{peak} is the applied shear stress at peak, σ'_n is the confining normal (effective) stress on the shear plane, dx is the incremental horizontal displacement at peak, dy is the incremental vertical displacement (expansion positive) at peak stress and μ is the friction coefficient. The energy dissipated by friction (the component in the right hand side) is equal to the sum of the work done by shearing (first component in the left hand side) and that needed to increase the volume (the second component in the left hand side). The latter component is referred to as dilatancy.

Rearranging equation (1.16),

$$\frac{\tau_{peak}}{\sigma'} = \tan \phi'_m = \mu + \left(\frac{dy}{dx} \right) \tag{1.17}$$

Thus, the peak shear stress ratio, or the peak mobilized friction angle ϕ'_m consists of both interlocking (dy/dx) and sliding friction between grains (μ). This equation that relates stress to dilation is called the stress-dilatancy rule, and it is an important relationship for characterizing the plastic deformation of soils.

Rowe (1962) recognized that the mobilized friction angle ϕ'_m must take into account particle rearrangements as well as the sliding resistance at contacts and dilation. Particle crushing, which increases in importance as confining pressure increases and void ratio decreases, should also be added to these components. The general interrelationships among the strength contributing factors and porosity can be represented as shown in Fig. 1.23. In this figure, ϕ'_f is the friction angle corrected for the work of dilation. It is influenced by particle packing arrangements and the number of sliding contacts. The denser the packing, the more important is dilation. As the void ratio increases, the mobilized friction angle decreases. The critical state is defined as the condition when there is no volume change by shearing (i.e.

---

[6] A number of additional useful correlations are given by Kulhawy and Mayne (1990).

(dy/dx) = 0 in equation (1.7)). The corresponding mobilized friction angle ϕ'_m is ϕ'_{crit}. The 'true friction' in the figure is associated with the resistance to interparticle sliding.

Critical state friction angle

The specific value of the critical state angle of internal friction ϕ'_{crit} depends on the uniformity of particle sizes, their shape, and mineralogy, and is developed at large shear strains irrespective of initial conditions. Typical values are 40º for well-graded, angular quartz or feldspar sands, 36º for uniform sub-angular quartz sand and 32º for uniform rounded quartz sand. Particle crushing appears to have little effect on ϕ'_{crit} (Coop, 1990; Yasufuku et al., 1991). This is demonstrated in the ring shear test results shown in Figs. 1.22(b) and (c); with increasing shear strains, the critical state strength is reached well before particle crushing ceases.

Peak friction angle

The peak friction angle can be considered as the sum of interparticle friction, rearrangement, crushing and the dilation contribution. For plane strain conditions, Bolton (1986) proposed the following empirical equation that relates the mobilized friction angle ϕ' at a given stress state to the critical state friction angle ϕ'_{crit} and dilation angle ψ.

$$\phi' = \phi'_{crit} + 0.8\psi \qquad (1.18)$$

where dilation angle ψ is the ratio of volumetric strain increment $d\varepsilon_v$ to the axial strain $d\varepsilon_1$ at the stress state of interest. This is similar to Taylor's equation (equation (1.16)). However, μ in equation (1.17) changes with shear, whereas ϕ'_{crit} is a constant material property.

The relative density D_r is a convenient index to characterize the interlocking characteristics packing structure. The effects of relative density, grain size, and gradation on the peak friction angle of cohesionless soils are illustrated by Fig. 1.24. Similar information in terms of void ratio, unit weight and Unified Soil Classification is given in Fig. 1.25. The peak values of friction angle for quartz sands range from about 30° to more than 50°, depending on gradation, relative density, and confining pressure.

Although the values of interparticle friction angle ϕ'_μ and the critical state friction angle ϕ'_{crit} are essentially constant for a given mineral, the magnitudes of the dilation angle ψ in equation (1.18) vary with effective confining pressure; that is, Figs. 1.24 and 1.25 apply for a particular value of confining pressure. In general, the contribution of dilation increases with increasing density and decreases with increasing confining pressure. The effect of confining pressure on peak friction angle is shown in Fig. 1.26 (Yamamuro and Lade, 1996). Up to confining pressures of 5 to 10MPa, the peak friction angle decreases with increasing confining pressure due to suppressed dilation and particle crushing. At pressures greater than about 10 MPa, the friction angle remains approximately constant, but the values in triaxial extension are smaller than those in triaxial compression.

To take effective confining pressure into account, Bolton (1986) proposed the normalized dilatancy index I_R, defined as

$$I_R = D_r(Q - \ln p') - R = D_r \ln\left(\frac{\sigma_c}{p'}\right) - R \qquad (1.19)$$

where D_r is the relative density, and p' is the mean effective confining pressure. The empirical parameter Q is related to the crushing strength of the soil particles; that is, $Q = \ln\sigma_c$, where σ_c is the crushing strength (same dimensions as p'). The Q values (using kPa) are 10 for quartz and feldspar, 8 for limestones, 7 for anthracite and 5.5 for chalk. Bolton (1986) found that R = 1 fits the available data well. The critical state is achieved when $I_R = 0$, and this is given as equation (1.15). I_R increases as the soil density increases. The parameter characterizes the state of the soil in relation to the critical state, similarly to the ones illustrated in Fig.1.22.

Using I_R (between 0 and 4), Bolton (1986) deduced the following correlations for the peak friction angle and critical state friction angle (in degrees) from the plots shown in Fig. 1.27.

$$\phi'_m - \phi'_{crit} = 3I_R \qquad \text{for triaxial compression conditions} \qquad (1.20)$$

$$\phi'_m - \phi'_{crit} = 5I_R \qquad \text{for plane strain conditions} \qquad (1.21)$$

The dilatancy contribution to sand strength, represented by the difference between the peak triaxial compression friction angle and the critical state friction angle ϕ'_{crit}, as determined by Bolton (1986), is shown in Fig. 1.28. The values shown are appropriate for quartz sands (Q = 10).

Other forms to characterize the peak friction angle in relation to the initial state of a sand are available. For example, Been and Jefferies (1986) relate the peak friction angle to the state parameter Ψ, defined in Fig. 1.22, as shown in Fig. 1.29.

1.5 Strength Parameters for clays

Friction angles

The peak value of ϕ' for clays decreases with increasing plasticity index and activity as shown in Fig. 1.30. Similarly, the critical state friction angle of normally consolidated kaolin clays ranges from 20 to 25 degrees, whereas that of montmorillonite clays is approximately 20 degrees. However, as the shearing continues, the friction angle of normally consolidated montmorillonite clays decreases to a value between 5 and 10 degrees. This is called the residual state. The friction angle of kaolin clays tends to remain near the above values even at large strains.

Failure envelope for overconsolidated clays

The differences in effective stress failure envelopes between normally consolidated and overconsolidated clays were illustrated in Fig. 1.3, and Hvorslev proposed the following relationship to model the strength characteristics of overconsolidated clays.

$$\tau_{ff} = c'_e + \sigma'_{ff} \tan \phi'_e \tag{1.22}$$

where ϕ'_e is an equivalent friction angle and c'_e is the cohesion intercept. These are called the Hvorslev parameters. If ϕ'_e is constant, c'_e becomes a linear function of σ'_e, which is the equivalent consolidation pressure as determined from the void ratio at failure e_{ff} as shown in Fig. 1.3.

$$c'_e = h_c \sigma'_e \tag{1.23}$$

where h_c is a material constant.

Substituting equation (1.23) into equation (1.22) gives

$$\frac{\tau_{ff}}{\sigma'_e} = h_c + \frac{\sigma'_{ff}}{\sigma'_e} \tan \phi'_e \tag{1.24}$$

Reported values of h_c and ϕ'_e range from 0.034 to 0.145, and from 9.9 to 18.8 degrees, respectively (Wood, 1990).[7]

Rearranging equation (1.24) gives

$$\tan \phi'_m \equiv \frac{\tau_{ff}}{\sigma'_{ff}} = h_c \frac{\sigma'_e}{\sigma'_{ff}} + \tan \phi'_e \tag{1.25}$$

where ϕ'_m is the mobilized friction angle at failure. For normally consolidated clay, (σ'_e/σ'_{ff}) =1 and $\tan\phi'_m = \tan\phi'_{crit} = h_c + \tan\phi'_e$. Substituting this into equation (1.25) gives

$$\tan \phi'_m = h_c \left(\frac{\sigma'_e}{\sigma'_{ff}} - 1\right) + \tan \phi'_{crit} \tag{1.26}$$

Hence the peak friction angle ϕ'_m for overconsolidated clays depends on the overconsolidation (σ'_e/σ'_{ff}) (the first term in the right hand side) and the critical state friction angle ϕ'_{crit}. The form of this equation is similar to equations (1.17) and (1.18) derived for sands.

---

[7] For general stress conditions, Schofield and Wroth (1968) modified the Hvorslev equation to the following.

$$\frac{q}{p'_e} = \frac{6 \sin \phi'_e}{3 - \sin \phi'_e} \left(c'_{pe} \cot \phi' + \frac{p'}{p'_e} \right) \quad \text{for triaxial compression}$$

$$\frac{q}{p'_e} = -\frac{6 \sin \phi'_e}{3 + \sin \phi'_e} \left(c'_{pe} \cot \phi' + \frac{p'}{p'_e} \right) \quad \text{for triaxial extension}$$

The Hvorslev parameters, ϕ'_e and c'_e, have been termed *true friction angle* and *true cohesion*, and are considered by some to reflect the mechanism of shear strength in terms of interparticle forces and friction. Such an interpretation is questionable, however, because two samples at the same water content but different effective stresses must have different structures. Thus, during deformation, there will be differences in volume change under drained conditions or differences in pore water pressure for deformation under undrained conditions. Furthermore, equation (1.23) shows that c_e' is an effective stress dependent property. Present evidence is that true cohesion is negligible in the absence of chemical bonding between particles caused by cementation.

Undrained shear strength

Undrained shear strength s_u coupled with total stress analysis ($c = s_u$ and $\phi = 0$ in equation (1.1)) is often used to examine the failure state of geotechnical structures under undrained conditions. The undrained shear strength of saturated normally consolidated clay determined using isotropically consolidated specimens as a function of liquidity index is shown in Fig. 1.31.

The undrained strength for a given initial void ratio e_{ini} can be obtained using the critical state equations (1.8) and (1.9).

$$s_u = \frac{M}{2}\exp\left(\frac{\Gamma - 1 - e_{ini}}{\lambda}\right) \tag{1.27}$$

The above equation applies to both normally consolidated and overconsolidated clays.

For a given soil, the initial void ratio e_{ini} can be related to the current stress state and the overconsolidation ratio. The relationship between undrained strength normalized by the effective over-burden stress after isotropic consolidation σ'_i has been deduced from critical state soil mechanics by Wroth and Houlsby (1985) as

$$s_u / \sigma'_i = 0.129 + 0.00435PI \tag{1.28}$$

in which PI is the plasticity index. Alternatively, the following relationship can be used for normally consolidated to slightly overconsolidated clays with low-to-moderate plasticity (Jamiolkowski et al., 1985)

$$s_u / \sigma'_{vp} = 0.23 \pm 0.04 \tag{1.29}$$

where σ'_{vp} is the vertical preconsolidation stress, and s_u is for direct simple shear.

The influence of overconsolidation on the undrained strength of clays is shown by Figs. 1.32 and 1.33. In Fig. 1.32, the undrained strength is normalized by the initial effective overburden pressure. In Fig. 1.33, the normalized strength of the overconsolidated clay is further normalized to the normalized strength of the normally consolidated clay. That normalization of undrained shear strength leads to unique relationships such as those in these figures forms the basis of the SHANSEP (Stress History and Normalized Soil Properties) method of design in soft clays (Ladd and Foott, 1974) that is widely used in practice.

$$\frac{s_u}{\sigma'_{v0}} = \left(\frac{s_u}{\sigma'_{v0}}\right)_{NC} (OCR)^m$$

where $(s_u / \sigma'_{v0})_{NC}$ is the strength ratio of normally consolidated clay, m is a material constant, and OCR is the overconsolidation ratio, defined as the ratio of the vertical preconsolidation stress σ'_{vp} to the current vertical stress σ'_v. Typical values of m range between 0.7 and 0.9. This method is particularly well suited for use with clays of low to medium sensitivity; i.e., clays that do not suffer large structural breakdown when consolidated beyond their preconsolidation pressure. It is also important to note that the strength ratio depends largely on the mode of shearing as shown in Fig. 1.34 (Ladd, 1991) and the values given in equations (1.28) and (1.29) are at the lower range (or the conservative side) in the figure.

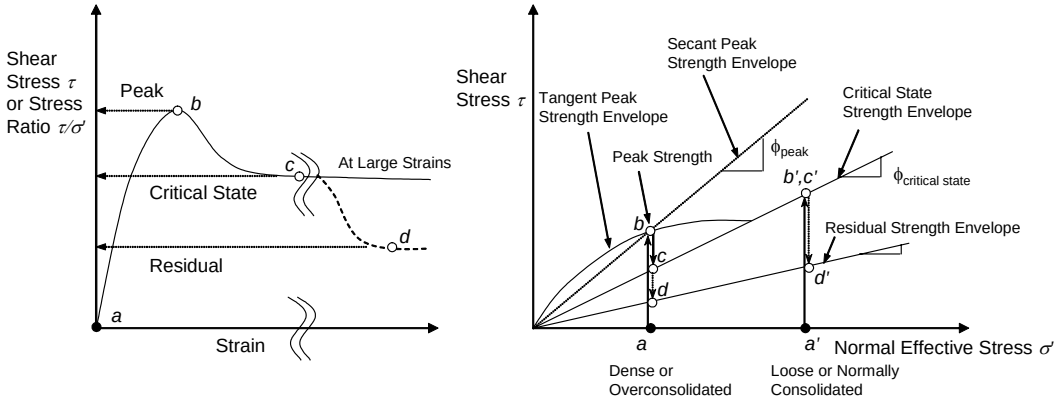

(a) (b)

Fig. 1-1

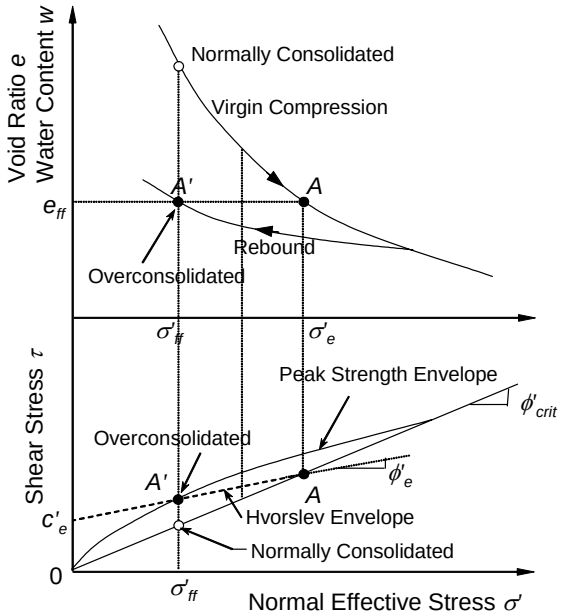

Fig. 1-2

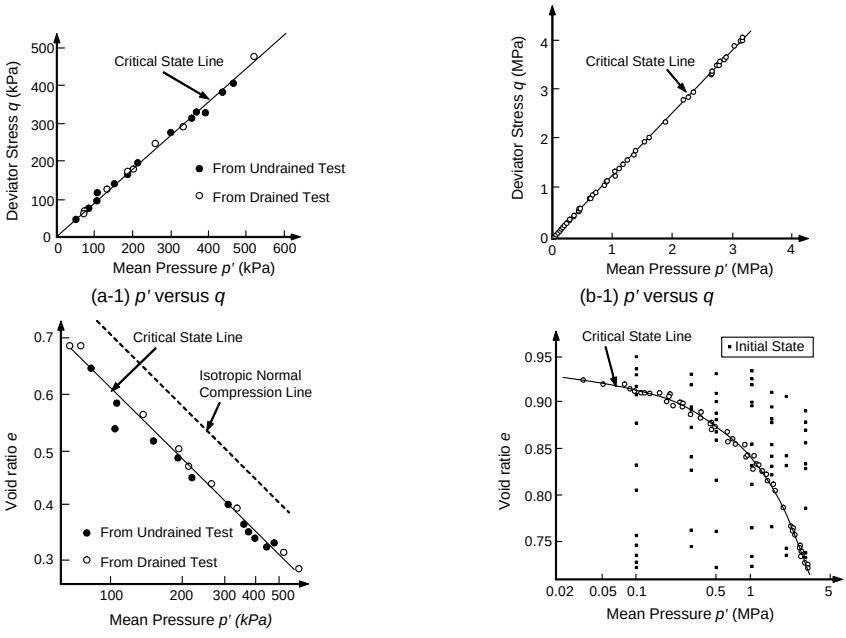

(a-1) p' versus q (b-1) p' versus q

(a-2) e versus lnp' (b-2) e versus logp'

(a) (b)

Fig. 1-3

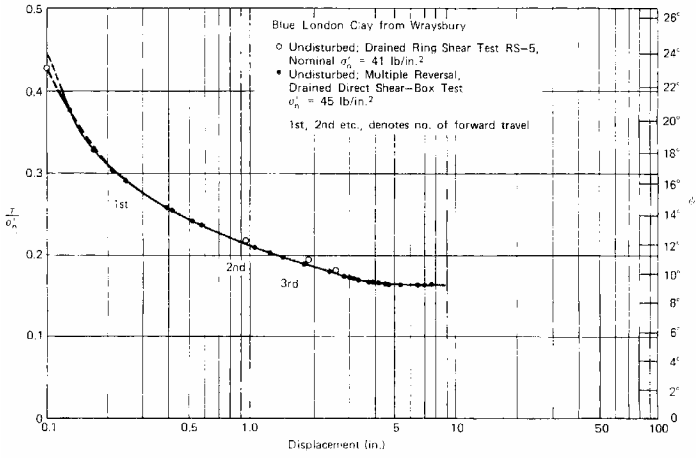

Fig. 1-4

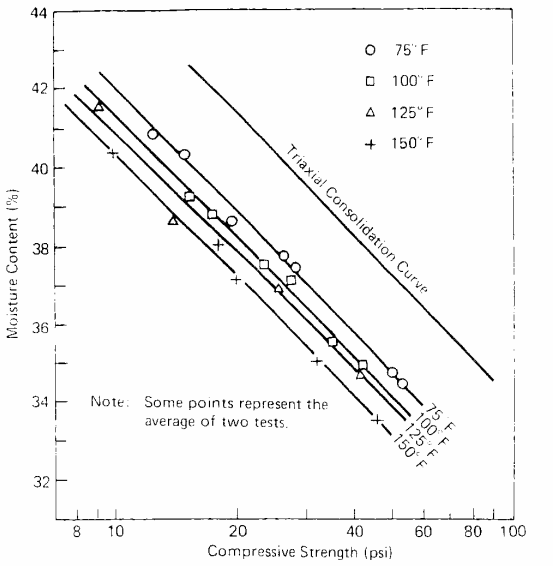

Fig. 1-5

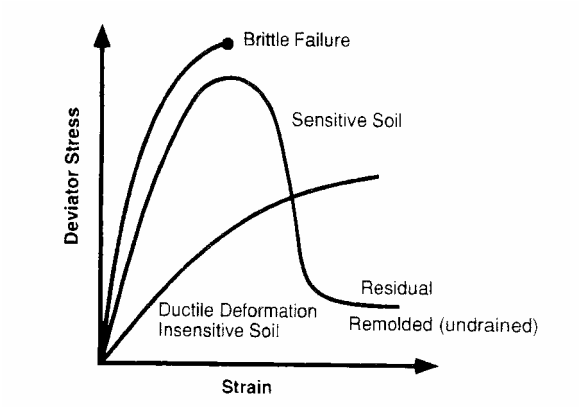

Fig. 1-6

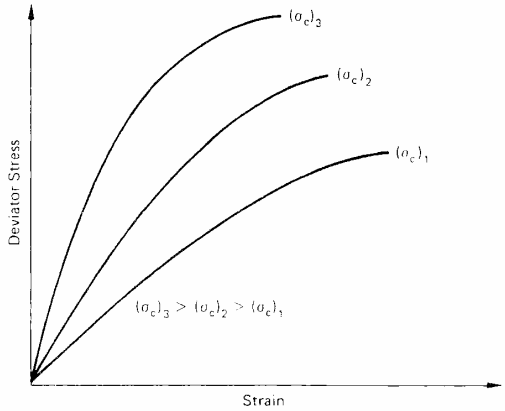

Fig. 1-7

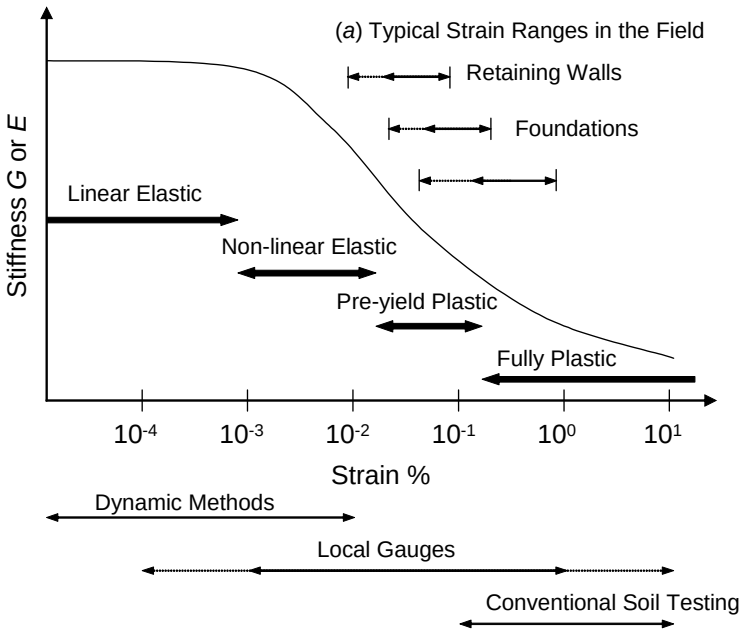

Fig. 1-8

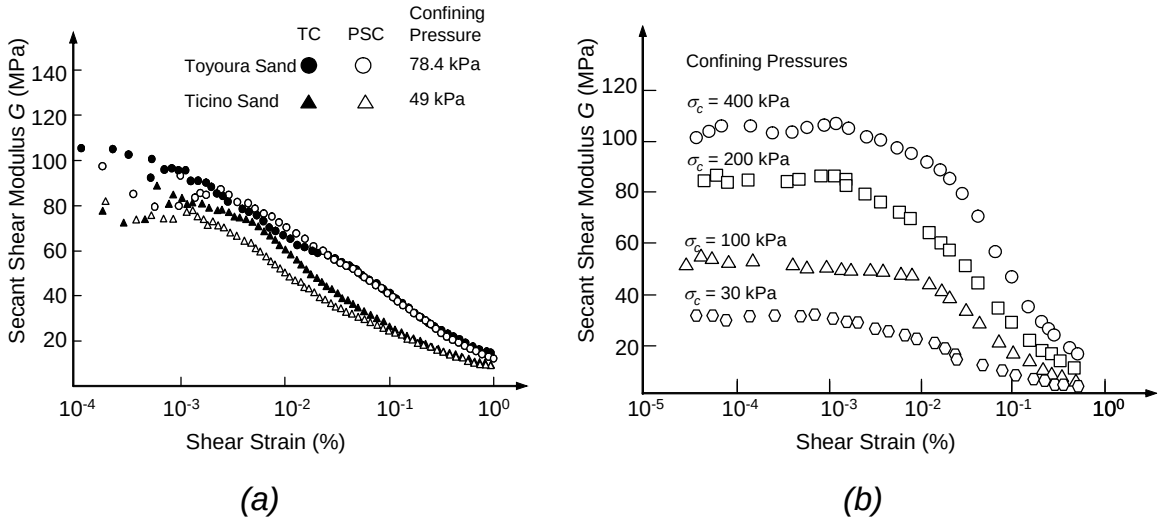

(a) *(b)*

Fig. 1-9

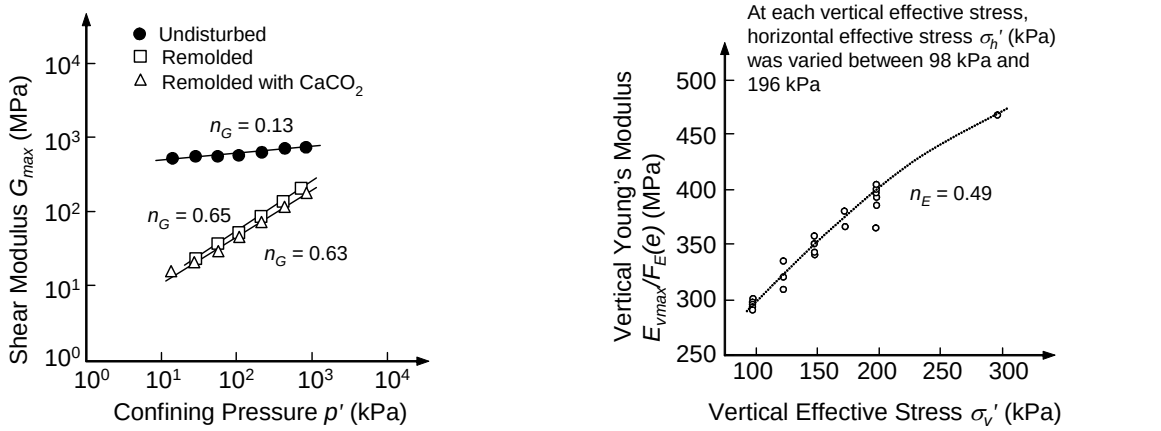

(*a*) (*b*)

Fig. 1-10

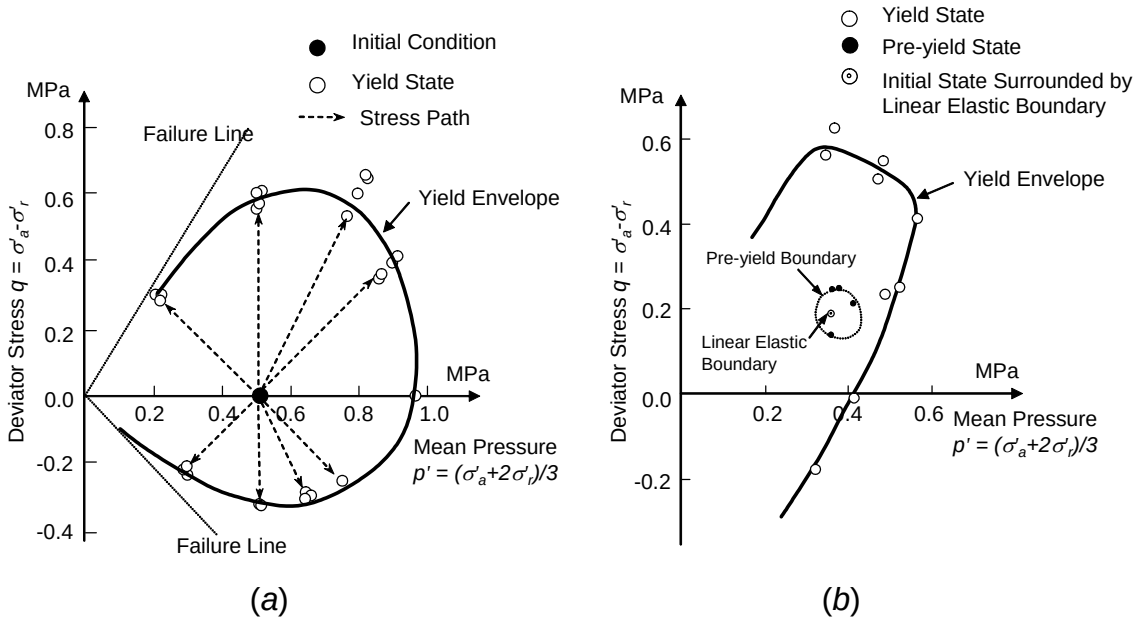

(*a*) (*b*)

Fig. 1-11

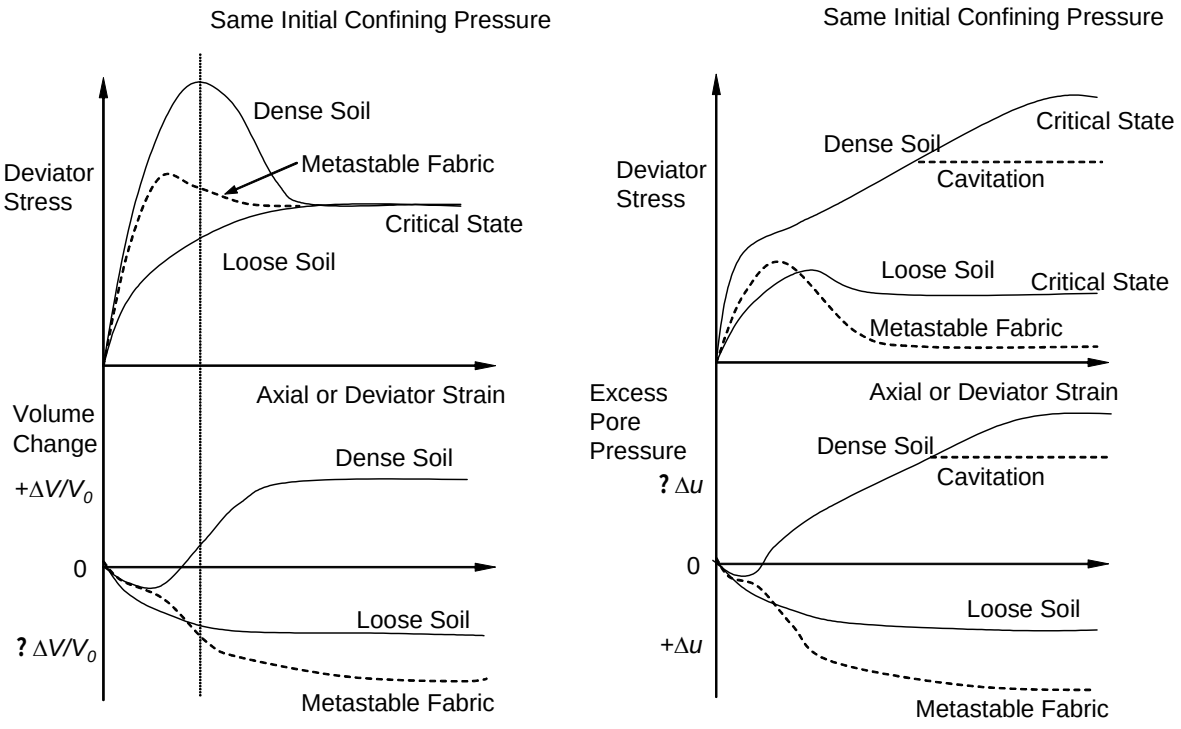

Fig. 1-12

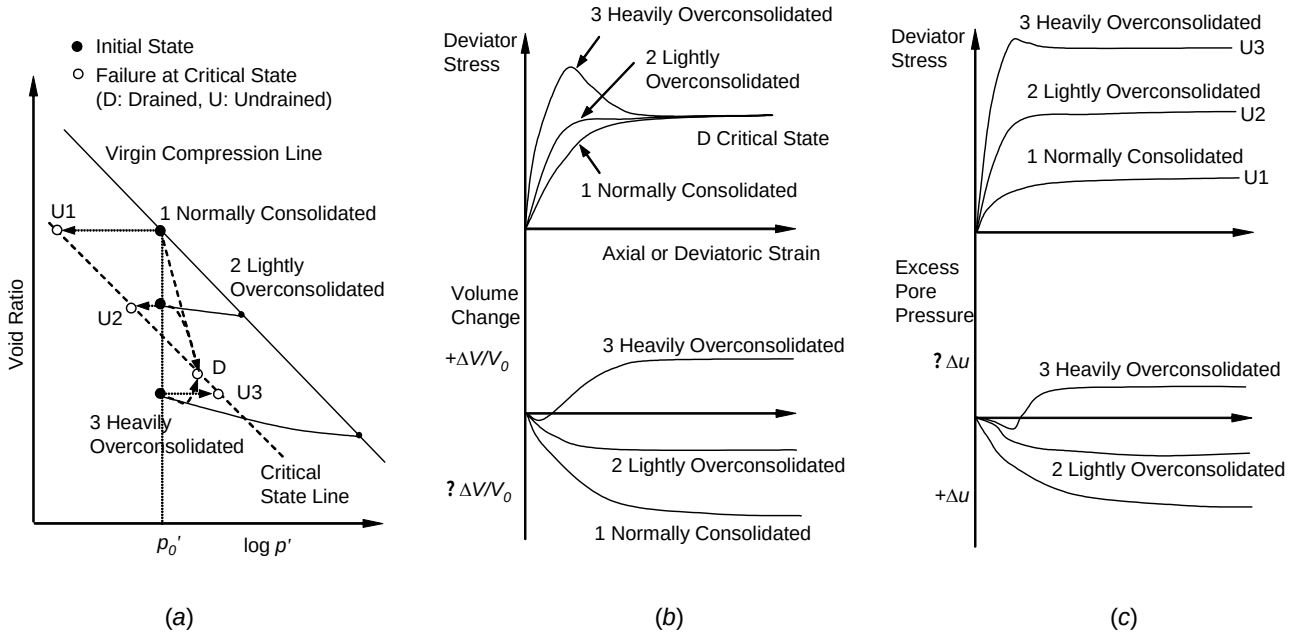

Fig. 1-13

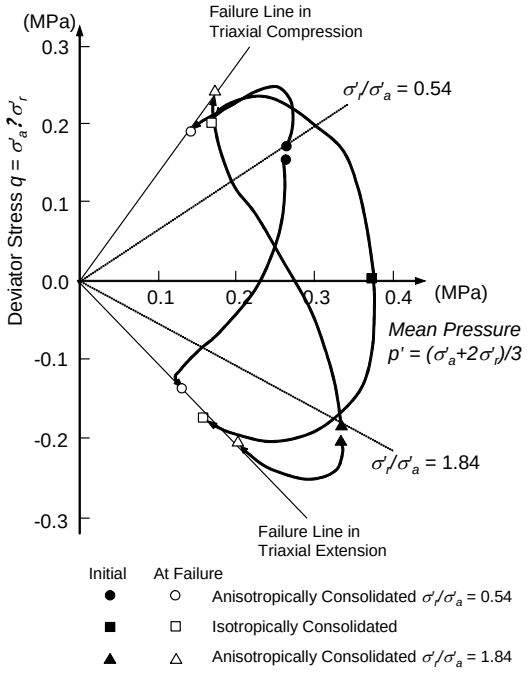

Fig. 1-14

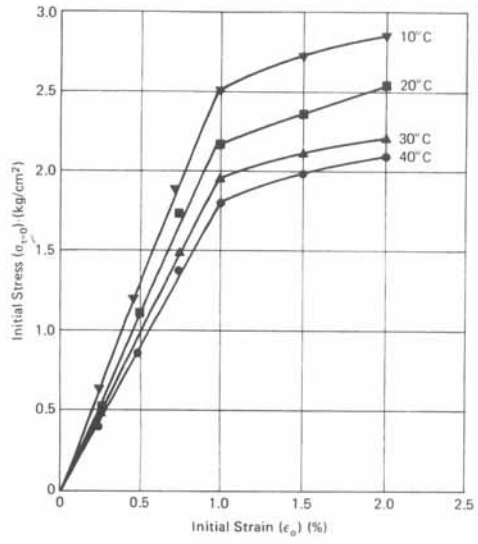

Fig. 1-15

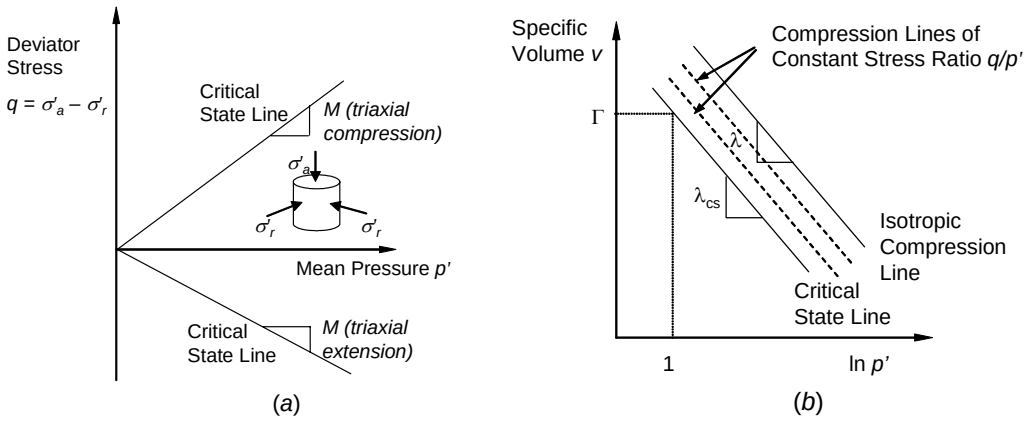

Fig. 1-16

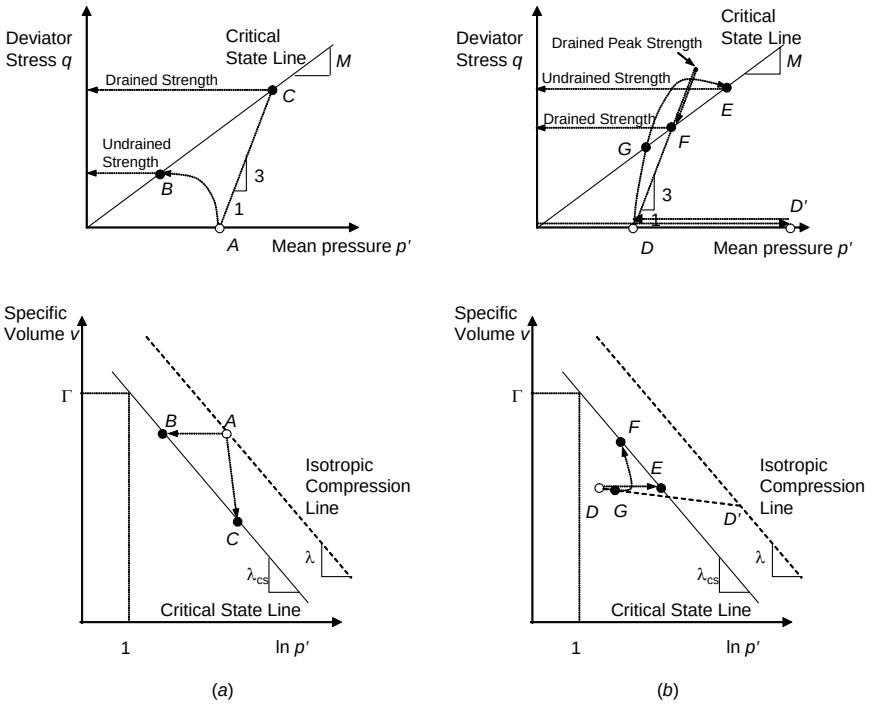

Fig. 1-17

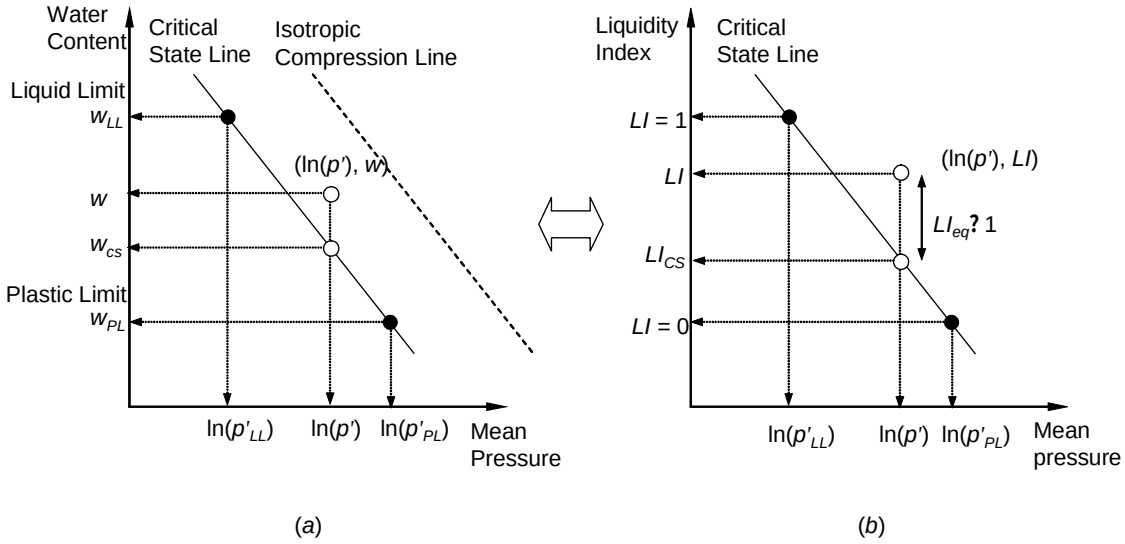

(*a*) (*b*)

Fig. 1-18

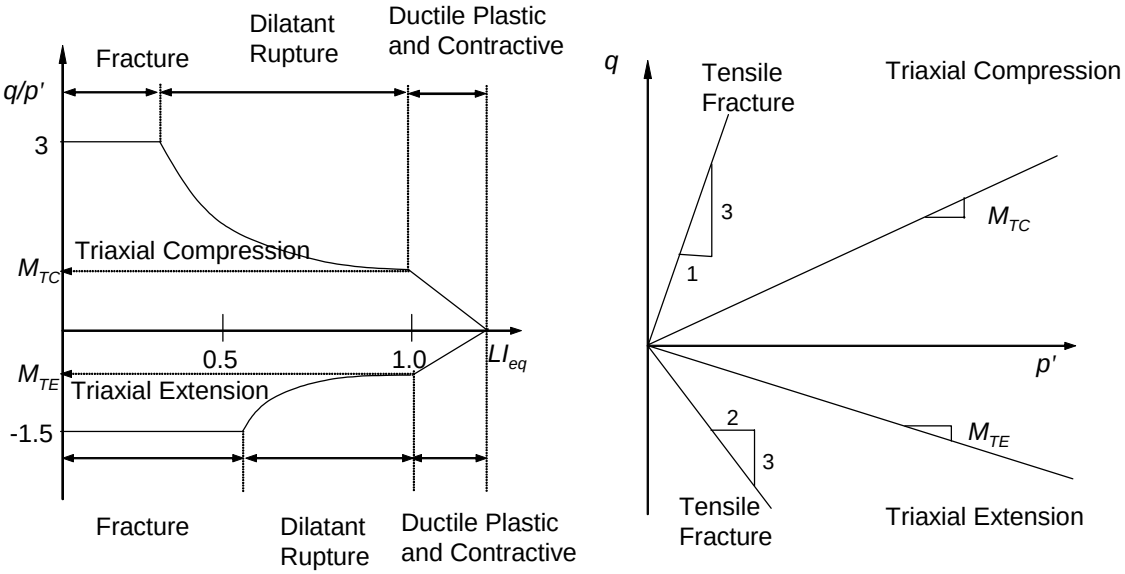

(*a*) (*b*)

Fig. 1-19

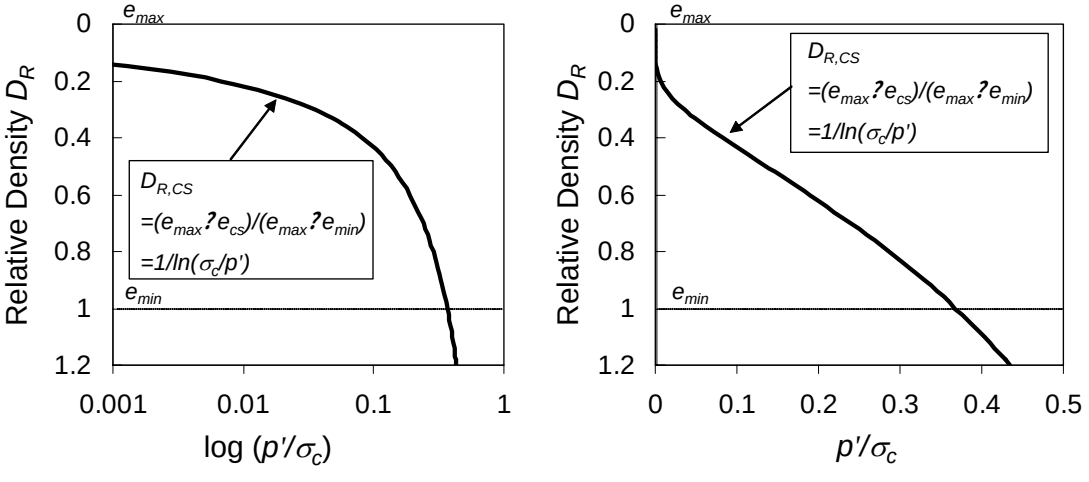

(*a*) (*b*)

Fig. 1-20

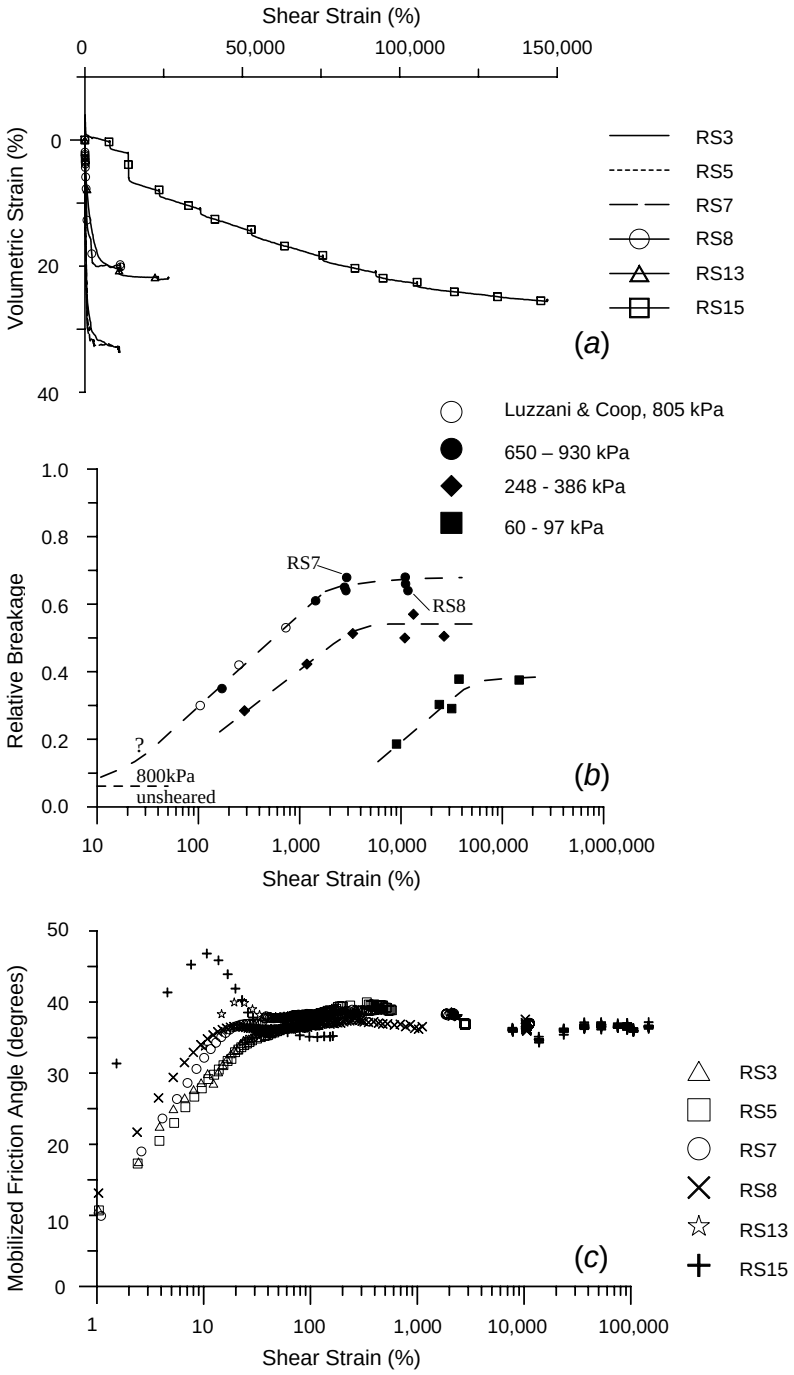

Fig. 1-21

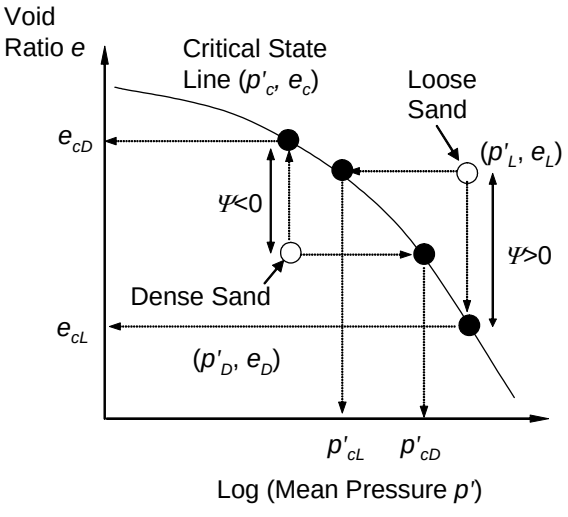

1. State Parameter (Been and Jefferies, 1985)

   $\Psi = e - e_c$

   Loose Sand $\Psi = e_L - e_{cL}$ (>0)

   Dense Sand $\Psi = e_D - e_{cD}$ (<0)

2. State Index (Ishihara et al., 1998)

   $I_s = (e_0 - e_c)/(e_0 - e)$

   Loose Sand $I_s = (e_0 - e_{cL})/(e_0 - e)$ (>1)

   Dense Sand $I_s = (e_0 - e_{cD})/(e_0 - e)$ (<1)

3. State Pressure Index (Wang et al., 2002)

   $I_p = p'/p'_c$

   Loose Sand $I_p = p'_L/p'_{cL}$ (>1)

   Dense Sand $I_p = p'_D/p'_{cD}$ (<1)

Fig. 1-22

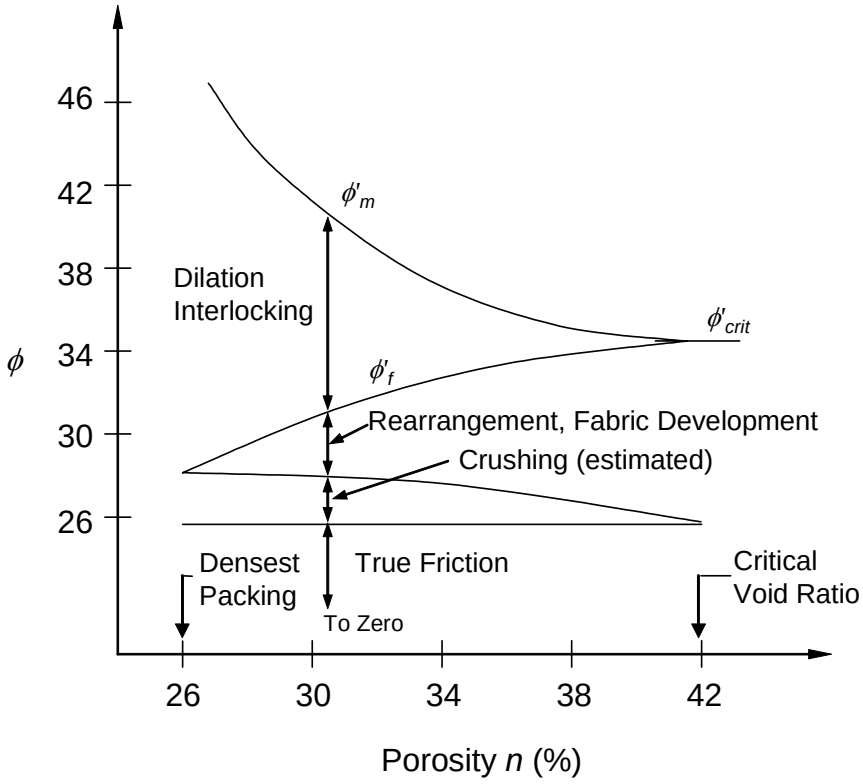

Fig. 1-23

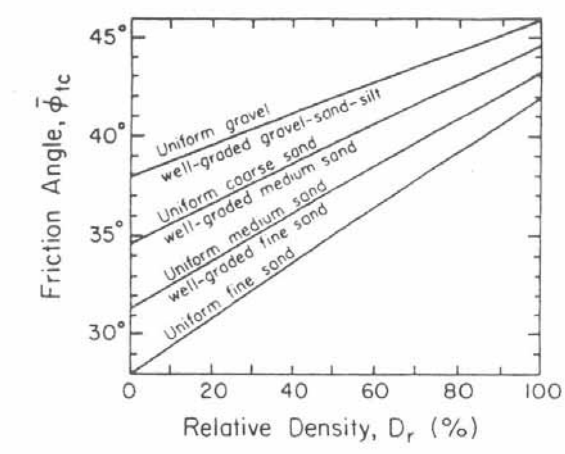

Fig. 1-24

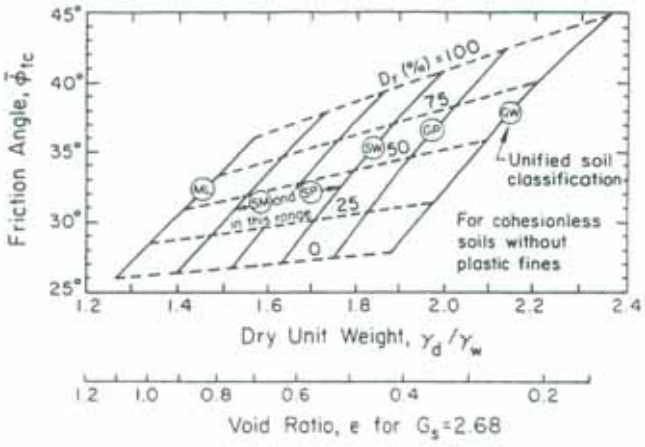

Fig. 1-25

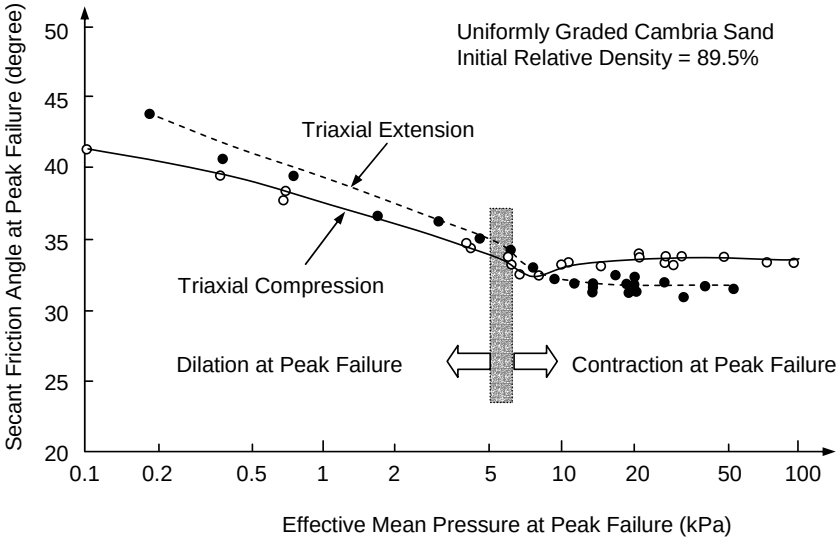

Fig. 1-26

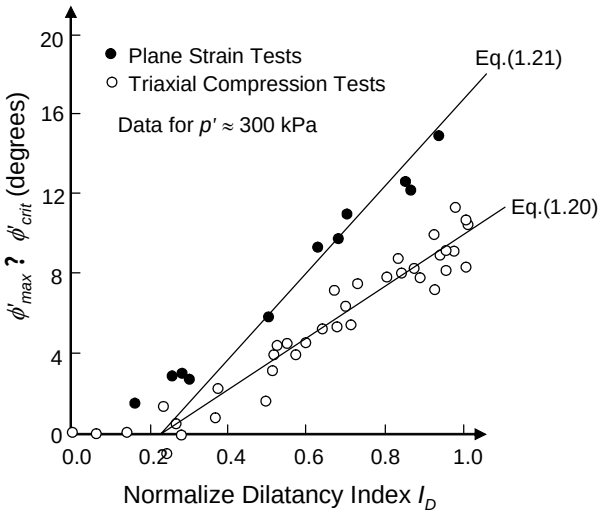

Fig. 1-27

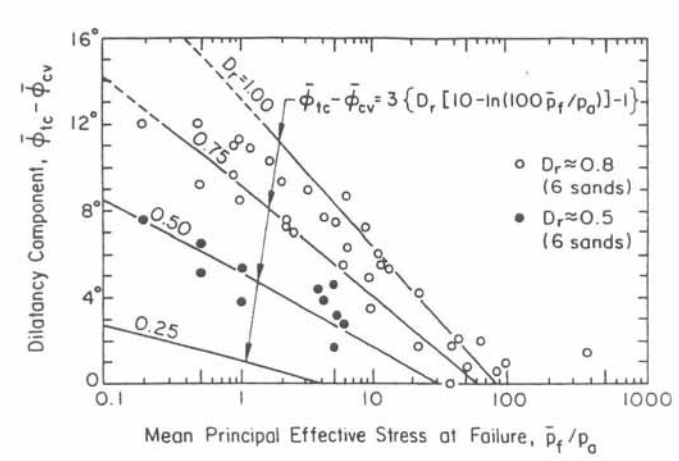

Fig. 1-28

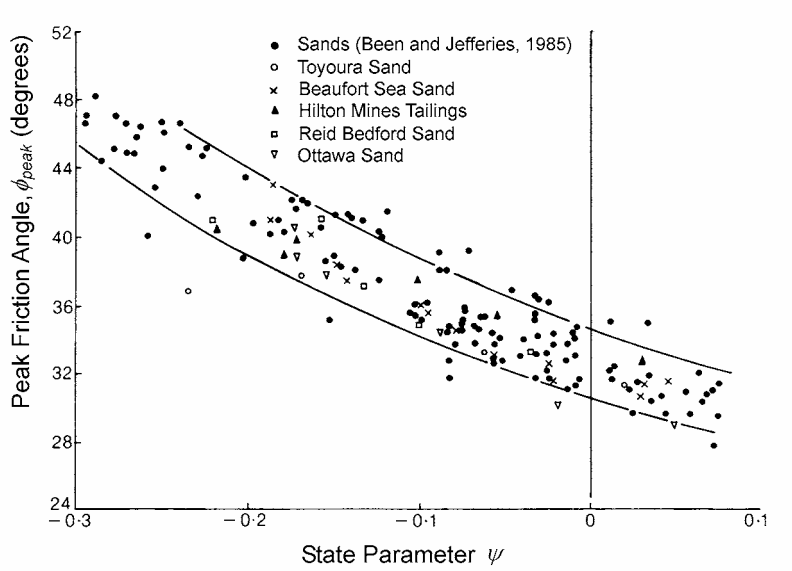

Fig. 1-29

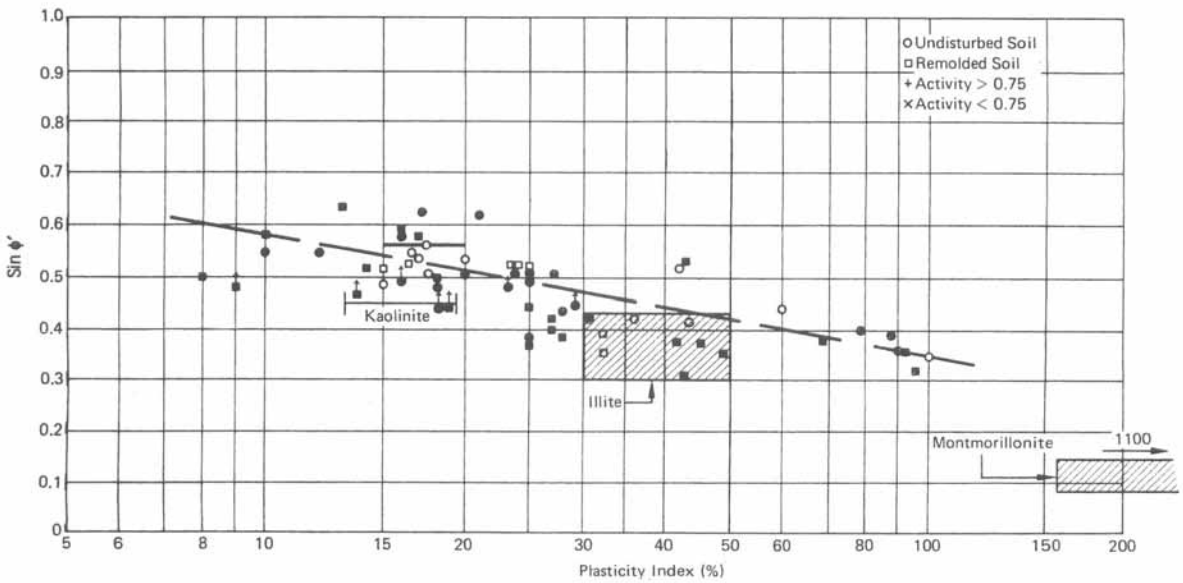

Fig. 1-30

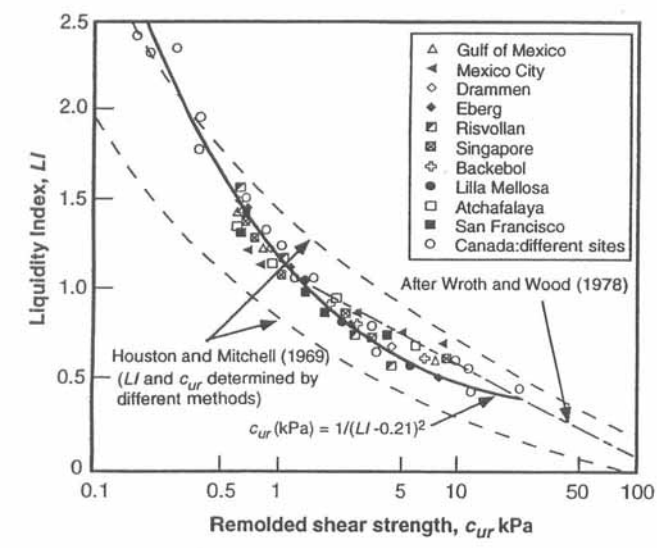

Fig. 1-31

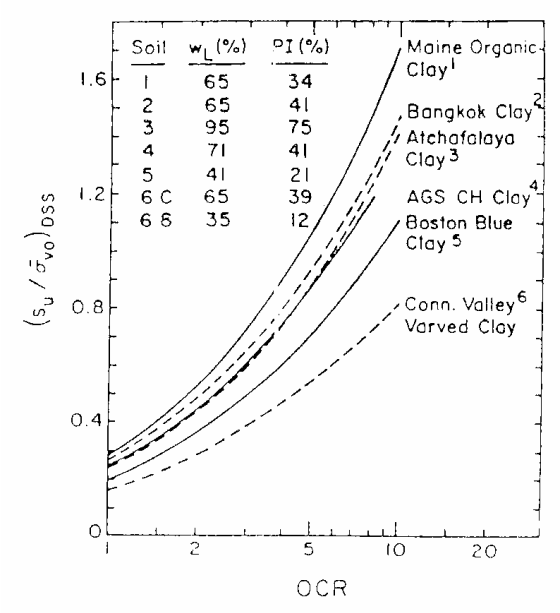

Fig.1-32

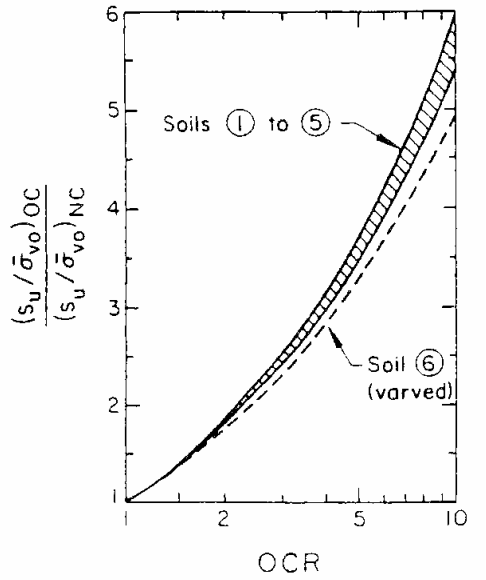

Fig. 1-33

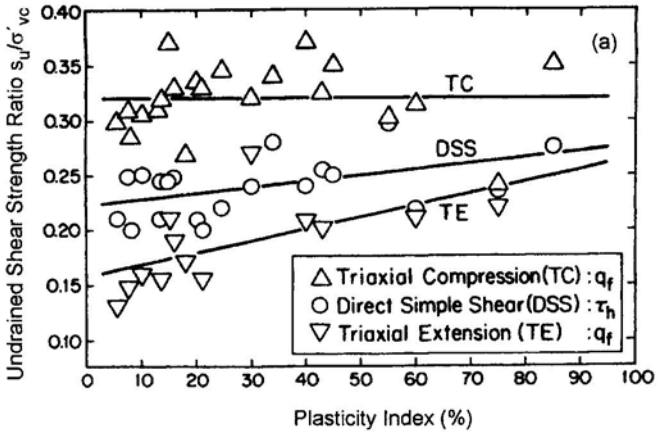

Fig. 1-34